ACS Sustainable Chemistry & Engineering

Research Article

pubs.acs.org/journal/ascecg

Understanding Multiscale Structural Changes During Dilute Acid Pretreatment of Switchgrass and Poplar

Sai Venkatesh Pingali,[*,†] Volker S. Urban,[*,†] William T. Heller,[†] Joseph McGaughey,[‡] Hugh O'Neill,[†] Marcus B. Foston,[∥,▽] Hongjia Li,[∥,#] Charles E. Wyman,[∥,#] Dean A. Myles,[†] Paul Langan,[†] Arthur Ragauskas,[∥,⊥] Brian Davison,[§,∥] and Barbara R. Evans[*,‡]

[†]Biology and Soft Matter Division, [‡]Chemical Sciences Division, [§]Biosciences Division and [∥]BioEnergy Science Center, Oak Ridge National Laboratory, P.O. Box 2008, Oak Ridge, Tennessee 37831, United States

[⊥]Department of Chemical and Biomolecular Engineering, University of Tennessee, 1512 Middle Drive, 419 Dougherty Engineering Bldg., Knoxville, Tennessee 37996, United States

[#]Department of Chemical and Environmental Engineering and Center for Environmental Research and Technology (CE-CERT), Bourns College of Engineering, University of California, 1084 Columbia Avenue, Riverside, California 92507, United States

[▽]Department of Energy, Environmental & Chemical Engineering, Washington University in Saint Louis, One Brookings Drive, Saint Louis, Missouri 63130, United States

Supporting Information

ABSTRACT: Biofuels produced from lignocellulosic biomass hold great promise as a renewable alternative energy and fuel source. To realize a cost and energy efficient approach, a fundamental understanding of the deconstruction process is critically necessary to reduce biomass recalcitrance. Herein, the structural and morphological changes over multiple scales (5−6000 Å) in herbaceous (switchgrass) and woody (hybrid poplar) biomass during dilute sulfuric acid pretreatment were explored using neutron scattering and X-ray diffraction. Switchgrass undergoes a larger increase (20−84 Å) in the average diameter of the crystalline core of the elementary cellulose fibril than hybrid poplar (19−50 Å). Switchgrass initially forms lignin aggregates with an average size of 90 Å that coalesce to 200 Å, which is double that observed for hybrid poplar, 55−130 Å. Switchgrass shows a smooth-to-rough transition in the cell wall surface morphology unlike the diffuse-to-smooth transition of hybrid poplar. Yet, switchgrass and hybrid poplar pretreated under the same experimental conditions result in pretreated switchgrass producing higher glucose yields (~76 wt %) than pretreated hybrid poplar (~60 wt %). This observation shows that other aspects like cellulose allomorph transitions, cellulose accessibility, cellular biopolymer spatial distribution, and enzyme−substrate interactions may be more critical in governing the enzymatic hydrolysis efficiency.

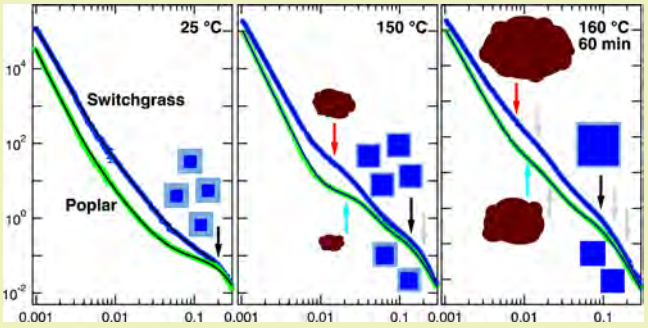

KEYWORDS: *Switchgrass, Hybrid poplar, Dilute acid pretreatment, Small-angle neutron scattering, Wide angle X-ray diffraction, Lignin aggregation*

INTRODUCTION

Lignocellulosic biomass has the potential to be an abundant and renewable feedstock for the production of second-generation bioethanol as well as numerous other fermentative products (e.g., other transportation fuels and chemicals).[1,2] Biomass feedstocks that are being considered as dedicated energy crops are comprised of two major categories: woody or herbaceous plants.[3] Recent attention in the United States has focused on the development of hybrid poplar[4] and switchgrass (*Panicum virgatum*) as the leading choices for high potential woody and herbaceous energy crops, respectively. Although these biomass feedstocks display many advantageous agronomic properties,[5−8] large-scale conversion operations will require a better understanding of their deconstruction and the differences occurring due to biomass source.

Lignocellulosic biomass cell wall chemistry, structure, and morphology evolved to withstand biochemical deconstruction, a property described as recalcitrance. As a result, efficient biochemical production of fermentable sugars from lignocellulosic biomass requires disruption of the plant cell wall by mechanical and/or chemical pretreatment.[9] Among the various thermochemical pretreatments, dilute sulfuric acid pretreatment with optimized high temperature−low residence times is one of the most attractive choices to increase enzymatic sugar yields because of its low cost, ease of application, and low propensity to cause sugar degradation and formation of inhibitory

Received: July 30, 2016
Revised: November 17, 2016
Published: December 5, 2016

DOI: 10.1021/acssuschemeng.6b01803
ACS Sustainable Chem. Eng. 2017, 5, 426−435

compounds.[9−11] Although the efficiency of cellulose enzymatic conversion to sugars is greatly increased by dilute acid pretreatment, improvements will increase the economic and life cycle viability of bioethanol production.[12] A large fraction of the research on dilute acid pretreatment of biomass for the bioethanol production has focused on understanding, modeling, and optimizing dilute acid pretreatment conditions to maximize sugar yields.[10] Though empirically useful at identifying trends, the conclusions of these studies can widely vary depending on the type of lignocellulosic biomass, scale of pretreatment, and reactor setup. Conversely, other research is concerned with elucidating the chemical, structural, and morphological changes to the cell walls of biomass during pretreatment, subsequently identifying mechanisms that result in increased enzymatic sugar yields.[11]

Over the years, this mechanistic research has shown that dilute acid pretreatments reduce biomass recalcitrance by altering cell wall properties at multiple levels: (1) chemical features, such as the hemicellulose content, the degree and type of linkages between lignin and hemicellulose, as well as the distribution of lignin monomer, monomer linkages, and terminal functional groups; (2) structural features, such as cellulose degree of polymerization and crystallinity; and (3) physical features, such as particle size, fiber modulus, and fiber length.[13] Current consensus suggests that these changes to the cell wall individually may have either a positive or negative effect on biomass recalcitrance but collectively reduce biomass recalcitrance through convoluted, complex, and nonlinear relationships. However, cellulose accessibility, as determined by the structure and morphology of the entire cell wall matrix, has emerged as a major first-order parameter affecting biomass recalcitrance.[14] Specifically, these studies have confirmed that lignin, whether native or in a modified and redistributed form following pretreatment, plays a major role in impeding access of enzymes (i.e., cellulases) to cellulose, resulting in inefficient enzymatic hydrolysis. For example, lignin was shown to nonproductively bind to family 1 type cellulose binding modules (CBMs) of both intact fungal cellulases CBH I (Cel7A), CBH II, and EGI and of CBM-GFP fusion proteins.[15] Also, lignin droplets, which formed and coalesced on cellulose surfaces as a result of pretreatment, were found to inhibit enzymatic digestion by blockage of enzyme access to the cellulose surface rather than through nonproductive binding to the enzyme.[16]

Previously, we employed small-angle neutron scattering (SANS) as a method to characterize changes in the cell wall structure and morphology of switchgrass simultaneously across multiple length scales (Å to submicrometer) during dilute acid pretreatment method.[17] Interestingly, we found that dilute acid pretreatment increased the cross-sectional diameter of the crystalline core of the cellulose fibril,[17] a finding that is contrary to the long-standing and well-cited belief that decrease in the crystallinity of cellulose is a major factor by which dilute acid pretreatment enables efficient enzymatic hydrolysis.[9] SANS also confirmed observation that dilute acid pretreatment leads to removal of hemicellulose, redistribution of lignin, and formation of lignin aggregates,[17] while uniquely providing dimensional information to describe these structural and morphological changes.[18] Among these molecular processes, the increase in the cross-sectional diameter of the crystalline core and lignin redistribution and aggregation are thought to reduce the conversion efficiency, whereas the removal of hemicellulose is believed to increase efficiency.[19,20]

Aside from changes in cellulose crystallinity, biomass recalcitrance has triggered investigations of lignin redistribution and aggregation on cellulose. Kraft lignin molecules in alkaline solutions self-associate to form compact colloidal particles, which eventually form a fractal supramolecular structure.[21] Conversely, Kraft lignin in aqueous salt solutions of NaCl or NaOH is observed to form elongated aggregates that are 1−3-nm-thick and 5−9-nm-long, but not at neutral pH.[22] During dilute acid pretreatment for deconstructing biomass, lignin molecules associate to form lignin droplets ranging from 5 nm to 10 μm as observed by electron microscopy.[23] Further, evidence of lignin rearrangement and relocalization was only observed at elevated temperatures, presumably above temperatures required for thermal transitions and/or depolymerization and repolymerization.[10,24,25] In addition, surface morphology of the lignin aggregates were determined to be highly irregular and folded, a structural feature that could promote unproductive binding of enzymes.[26] Therefore, the role of lignin in recalcitrance has driven the development of genetically engineered plants using iRNA and other recombinant DNA techniques to target specific biosynthetic genes;[27,28] for example, transgenic switchgrass with reduced lignin content and altered monolignol distribution showed an increase of up to 38% in ethanol yield by conventional biomass fermentation processes.[29]

In this paper, we report the use of scattering studies to specifically understand structural changes to cellulose and lignin during dilute acid pretreatment to sugar yields and ultimately provide valuable scientifically driven strategies to improve cellulosic biofuel production.

MATERIALS AND METHODS

Sample Preparation. Samples of the lowland cultivar Alamo switchgrass (*Panicum virgatum*) were harvested and provided by the Samuel Roberts Noble Foundation in Ardmore, OK. Poplar hybrid (*Populus trichocarpa* x *deltoides*) clonal samples were harvested between 2007 and 2008 at area 0800 at Oak Ridge National Laboratory, TN and debarked. For details of sample storage and removal of extractives, refer to the Supporting Information.

Preparation of Dilute Acid Pretreated Samples. Dilute acid pretreatment of switchgrass and hybrid poplar was carried out by a modification of reported methods.[30,31] **Untreated (P0)**: The sample was Wiley milled and extracted. **Presoak (P4)**: Wiley milled biomass samples were presoaked at room temperature (25 °C) while continuously stirring in a ∼1% dilute sulfuric acid solution at 5% dry solids (w/w) for 4 h. The presoaked slurry was filtered, and the solid material was washed with an excess of deionized water to prepare sample P4 or further treated as follows. **Ramp-up (R50, R75, R100, R125, R150)**: The presoaked material was transferred to a 4560 mini-Parr 300 mL pressure reactor of Parr Instrument Company in a ∼1% (or 0.1−0.2 M) dilute sulfuric acid solution at 5% solids (w/w) and sealed. The impeller speed was set to ∼100 rpm, and the vessel was heated to 160 °C for ∼30 min (at ∼6 °C/min). **Constant (C2, C5, C10, C20, C60)**: The reactor was kept at 160 ± 2 °C (6.4−6.8 atm) for the specified residence time: 2, 5, 10, 20, and 60 min (±0.5 min). All yields for biomass recovered after pretreatment ranged between 75 and 85% by mass of the initial material. To halt the pretreatment process to obtain ramp-up and constant samples, the reactor was quenched in an ice bath (1−5 min to cool to 70 °C) at different temperatures during ramp-up. Then, the pretreated slurry was filtered to remove the solid residue and washed with an excess of deionized water and dried overnight at room temperature.

Preparation of Lignin-Extracted Samples. Lignin extraction of biomass samples was performed by methods previously used for preparation of hybrid poplar samples for NMR analysis.[32] Dilute acid pretreated samples (1.5 g) were dispersed in 125 mL of deionized

DOI: 10.1021/acssuschemeng.6b01803
ACS Sustainable Chem. Eng. 2017, 5, 426−435

water in a Kapak sealing pouch. The resulting mixture was heated in a water bath for 1 h at 75 °C prior to adding 1 mL of glacial acetic acid and 1 g of sodium chlorite ($NaClO_2$) and continuing the reaction for an additional 1 h. This procedure was repeated three times to give a total treatment time of 3 h. The treated sample was then quenched in ice-water, filtered, and washed thoroughly using deionized water and acetone before finally being air-dried overnight.

Small-Angle Neutron Scattering (SANS). SANS measurements were performed with the CG-3 Bio-SANS instrument[33] at the High Flux Isotope Reactor (HFIR) facility of Oak Ridge National Laboratory. All samples were exchanged in fresh 100% D_2O solvent three times in a span of about 24 h to maximize D/H exchange and solvent penetration. Soaked samples were placed in 0.5-mm-thick quartz cells with detachable cell walls (Hellma Model# 106-QS 0.5MM rectangular cell and 124-QS 0.5MM circular cell) for SANS studies. Three different instrument configurations were employed to collect data over the range of scattering vectors, 0.001 $Å^{-1} < Q < 0.3$ $Å^{-1}$, and more details are included in the Supporting Information. Scattering profiles $I(Q)$ versus Q were analyzed using a multilevel unified fit implemented in the Irena Package[34] to elucidate the multiple levels of structural organization. Examples of these fits include polymers[35] and hierarchically structured lignocellulosic biomass.[17]

Wide-Angle X-ray Diffraction (WAXD). WAXD measurements were performed using a theta−theta goniometer Bruker D5005 instrument using Cu Kα radiation (λ = 1.542 Å) operating at 40 keV and 40 mA. The sample-holder was a flat glass slide with a circular trough in the center for the sample. Using Bragg's law and Scherrer equations,[36,37] d-spacing and crystallite sizes, respectively, were obtained by employing a peak fitting method, and more details are provided in the Supporting Information.

Scanning Electron Microscope (SEM). All samples were mounted onto a stage and then coated with gold for 2 min by EM350 sputter. Images were acquired *via* a JEOL-1530 Thermally-Assisted Field Emission (TFE) Scanning Electron Microscope (SEM) at 12 or 10 kV at various resolving powers.

Compositional Analysis. Glucan and xylan contents were determined by performing a downscaled compositional analysis method[38] that is nearly identical to conventional wet chemistry procedures[39] but uses 100 times less biomass. The entire process was performed in 1.5 mL high recovery glass vials (Agilent, Santa Clara, CA, USA), and 3 mg of dry biomass was loaded into each vial by an automation robotics platform (Symyx Technologies, Sunnyvale, CA). Sugars were analyzed by Waters Alliance 2695 HPLC (Milford, MA, USA) equipped with an Aminex HPX-87H column (BioRad, Hercules, CA, USA) and a refractive index detector. The residual acid insoluble material was considered the lignin content.

Enzymatic Hydrolysis. The high throughput enzymatic hydrolysis method is based on the High Throughput Pretreatment and Enzymatic hydrolysis (HTPH) design at University of California, Riverside.[40,41] In this particular study, an automation robotics platform (Symyx Technologies, Sunnyvale, CA) was used to perform batch enzyme hydrolysis; refer to the Supporting Information for details such as enzyme loading and sugar quantifications.

RESULTS

SANS scattering curves of switchgrass and hybrid poplar for different dilute acid pretreatment times are shown in Figure 1 (see Figures S1 and S2 for more details). Structural features of all the curves clearly show three main structural regimes: *Pri* for primary ($Q > 0.06$ $Å^{-1}$), *Sec* for secondary (0.006 $Å^{-1} < Q <$ 0.06 $Å^{-1}$), and *Ter* for tertiary (0.001 $Å^{-1} < Q < 0.006$ $Å^{-1}$). The solid black lines are the unified fit[42,43] results. Every structural feature or regime corresponds to a level of the unified fit. We observe an exponential feature, indicative of a characteristic length scale, for all the curves in the primary regime and a power-law feature for all the curves in the tertiary regime. The secondary regime, enlarged for clarity in Figure S1, exhibits different features at the various stages in the pretreatment process. Curves P0 and R125 exhibit a power-law character, while curves R150, C2, and C60 exhibit exponential character. SAS data, especially of dense, complex materials, may represent all kinds of coherent scattering length density fluctuations, and an interpretation can be misleading. Over multiple structural levels, the unified fit approach

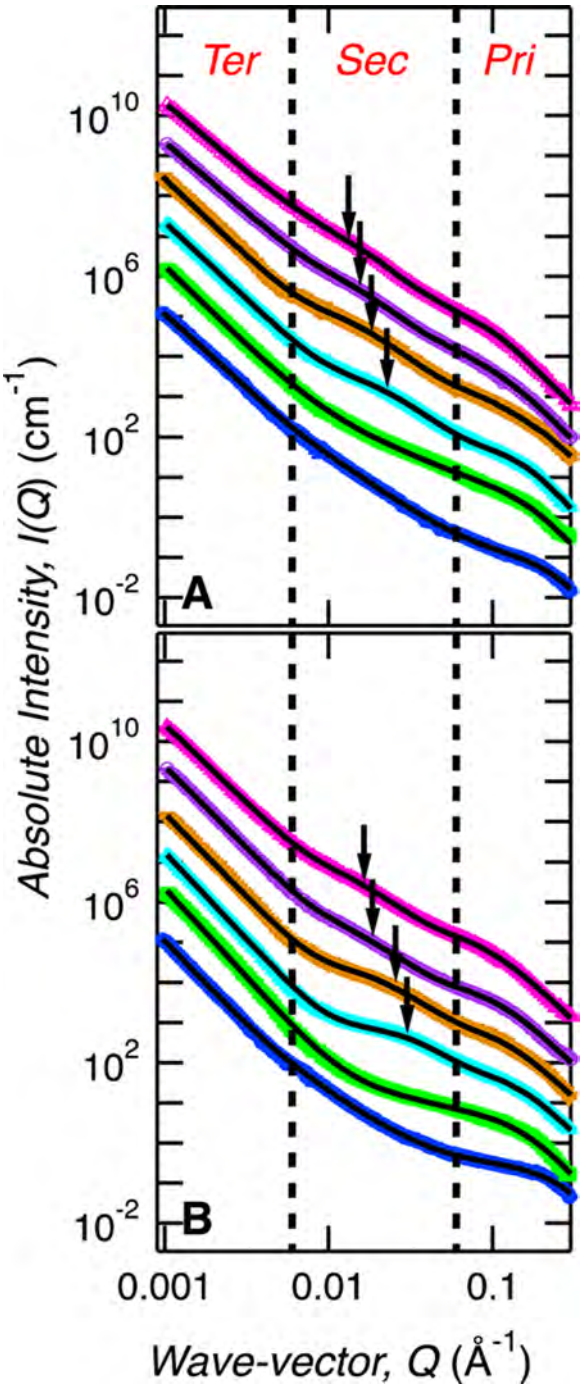

Figure 1. SANS curves of dilute acid pretreated (A) switchgrass and (B) hybrid poplar samples. The curves represent (*i*) native, P0 (blue dots); dilute acid pretreatment at (*ii*) 125 °C, R125 (filled green squares); and (*iii*) 150 °C, R150 (filled light blue top triangle) of the ramp-up phase; dilute acid treated at 160 °C for (*iv*) 2 min, C2 (filled orange down triangle); (*v*) 20 min, C20 (open purple circles); and (*vi*) 60 min, C60 (open pink top triangle). The solid black lines are the unified fit to the experimental SANS data. All of the curves (except native) have been offset for clarity.

DOI: 10.1021/acssuschemeng.6b01803
ACS Sustainable Chem. Eng. 2017, 5, 426−435

deconvolutes average size, radius of gyration, and correlation between structural units as expressed by power laws. We are confident that our approach provides valuable information, especially as part of the body of work that includes the use of many techniques. We have used NMR and compositional analysis,[32,59] fiber diffraction and computation,[67] microscopic studies, and enzymatic digestion; all these studies corroborate our interpretation of SANS data. Assuming validity of this structural model, the unified fit provides a minimal set of parameters that describe the hierarchical structure.

Figure 1A summarizes the structural and morphological trends of switchgrass during dilute acid pretreatment obtained by SANS. First, the characteristic features in the primary regime shifts progressively to smaller Q, which indicates an increase in size. Second, the slope (or the power-law exponent) in the tertiary regime decreases after long reaction times at 160 °C. Third and final, a power-law behavior at 125 °C transforms to an exponential at 150 °C in the secondary regime (see Figure S1A). The same set of trends as described above is observed for hybrid poplar (Figure 1B). Furthermore, native samples of both switchgrass and hybrid poplar have a similar location in the Q-scale of the exponential feature in the primary regime and slope of the power-law feature in the secondary regime. A more detailed comparison of switchgrass and hybrid poplar reveals three clear differences. First, the shift of the exponential feature toward small-Q in the primary regime is larger for switchgrass. Second, at 125 °C, the slope in the secondary regime is greater for switchgrass than that for hybrid poplar. Third and finally, at or above 150 °C, the location in Q-scale of the exponential feature for switchgrass shifts to smaller-Q than it does for hybrid poplar.

Figure 2 summarizes the trends in the fit parameters of the multilevel unified fit, such as radius of gyration R_g and power-law exponent P. The two distinct sizes (R_g) of the structural signatures observed are attributed to lignin aggregates in the secondary regime[17] and cellulose fibril diameter in the primary regime, respectively.[17,44] Lignin aggregates appear abruptly at 150 °C (Figure 2C), and the initial size of the aggregates as observed for switchgrass is much larger ($R_g \sim 90$ Å) than those in hybrid poplar ($R_g \sim 55$ Å). However, lignin aggregate size, for both herbaceous and woody plants, grows 2-fold after treatment for 60 min at 160 °C. With regard to cellulose fibril diameter, native samples of both switchgrass and hybrid poplar have the same average cellulose fibril diameter. But, after 60 min at 160 °C, a 4-fold increase was observed for switchgrass (9 to 36 Å) and 2-fold for hybrid poplar (9 to 22 Å), see Figure 2B (and Tables S1 and S2).[17,44] Other structural features extracted include surface and bulk morphologies obtained from the power-law exponents. The surface morphology of the micron-sized cell walls shows a reduction in the power-law exponent for both switchgrass and hybrid poplar samples (tertiary regime of Figures 1 and 2D). For switchgrass, the cell wall surface characteristics transitions from a smooth to a crumpled surface ($P \sim 4.0$ to 3.5), while hybrid poplar transitions from a diffuse interface[17,45] to a smooth surface ($P \sim 4.5$ to 4.0). The scattering profiles in the secondary regime initially exhibit a power-law behavior that eventually transitions to a particle size by 150 °C (Figures 1 and S1). Below 150 °C, the exponent of the power-law behavior represents a mass-fractal, which characterizes the conformation or degree of branching of the biopolymers in the system. Both native samples have a highly branched biopolymer network ($P \sim 2.5$) around room temperature, which abruptly breaks down on heating in dilute

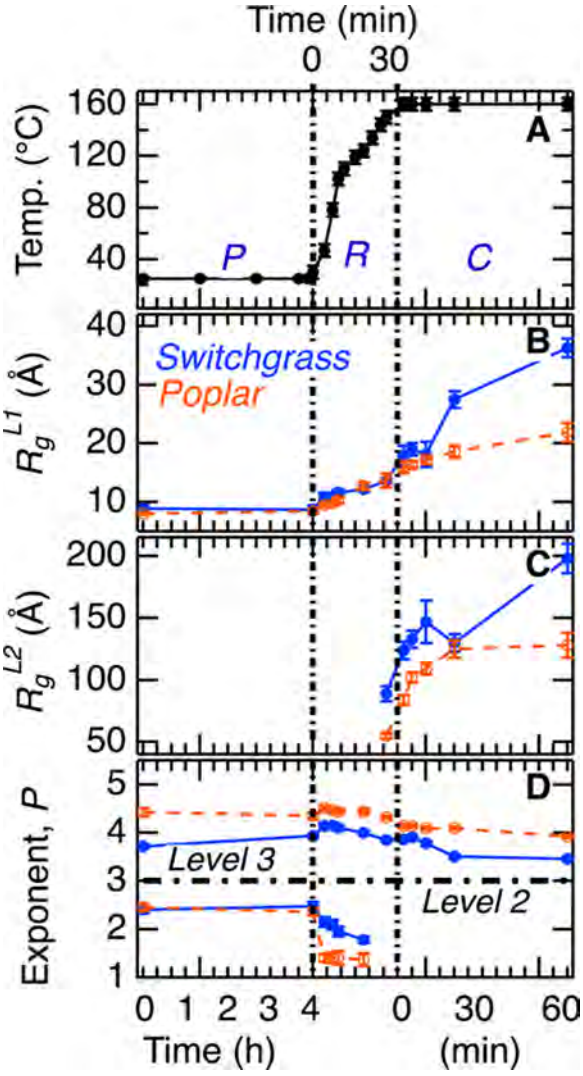

Figure 2. Reaction temperature (A) and unified fit parameters as a function of dilute acid pretreatment progress. Unified parameters are (B) cellulose fibril radius of gyration, R_g^{L1} (Å), (C) lignin aggregate radius of gyration, R_g^{L2} (Å), and (D) mass (level 2) or surface (level 3) fractal dimension, P. The reaction time is divided into three sections, P for presoak phase monitored in hours, R for ramp-up, and C for constant phases were monitored in minutes. Samples studied are switchgrass (orange open circles) and hybrid poplar (blue dots).

sulfuric acid indicated by a decrease in the exponent.[17] The reduction in the degree of branching is greater for hybrid poplar (2.5 to 1.4) than for switchgrass (2.5 to 1.8).

We performed a sodium chlorite lignin extraction process on some representative switchgrass and hybrid poplar samples taken at different stages of pretreatment. Tables S1 and S2 list the unified fit results of those samples. The lignin extraction process[32,46] removes lignin with minimal disruption to the cellulose structure. Therefore, removal of the lignin aggregates exposes the underlying cellulose fibril bulk morphology, which is characterized by the power-law behavior in the secondary regime. The exponent for the dilute acid pretreated switchgrass samples (2 and 10 min at 160 °C) after lignin extraction is in good agreement with the exponent at 125 °C ($P \sim 1.8$) just prior to the appearance of the lignin aggregates (150 °C). In pretreated hybrid poplar (2 and 10 min at 160 °C), lignin extraction shows a slightly larger exponent ($P \sim 1.6$–1.8) than

DOI: 10.1021/acssuschemeng.6b01803
ACS Sustainable Chem. Eng. 2017, 5, 426−435

at 125 °C ($P \sim 1.4$). Even with the slightly larger exponent for hybrid poplar, the basic underlying cellulose fibril network can be considered to undergo slightly more opening of the structure as the reaction progresses from 125 °C to 10 min pretreatment at 160 °C. Importantly, other structural features, such as the cellulose fibril diameter (primary regime) and the surface morphology of the micron-sized cell walls (tertiary regime), do not undergo significant change when lignin is extracted. This finding is consistent with the mild nature of the chosen lignin extraction process[32,46] that does not affect the underlying cellulose fibril hierarchical structure.

To further probe cellulose microfibril structure, wide-angle X-ray diffraction data (WAXD) were obtained from switchgrass samples (Figures S2). The values of d-spacing, d_{200}, and crystallite thickness, L_{200}, obtained from peak center and fwhm of diffraction peak (200) are listed in Table 1. Peak (200) with

Table 1. WAXD Results of Dilute Acid Pretreatment of Switchgrass

	center$_{200}$	peak$_{200}$ fwhm	d spacing	crystallite thickness
samples	2θ (deg)	$\beta_{1/2}$ (deg)	d_{200} (Å)	L_{200} (Å)
P0	22.03 ± 0.05	3.4 ± 0.1	4.03 ± 0.01	24.1 ± 0.8
dilute acid pretreated				
P4	21.89 ± 0.07	3.4 ± 0.2	4.06 ± 0.01	24.0 ± 1.7
C2	22.48 ± 0.04	2.0 ± 0.2	3.96 ± 0.01	40.7 ± 3.1
C5	22.42 ± 0.04	2.1 ± 0.1	3.97 ± 0.01	39.3 ± 2.7
C10	22.48 ± 0.06	2.0 ± 0.2	3.96 ± 0.01	41.2 ± 3.2

$2\theta \sim 22.5°$ represents correlations between alternate cellulose planes of cellulose strands[47−49] and probes the average crystalline order perpendicular to the fibril axis. The position of peak (200) has shifted to higher angles (2θ), or equivalently, d-spacing has decreased from 4.06 to 3.96 Å due to dilute acid pretreatment between stages P4 and C2. Furthermore, peak (200) becomes sharper from P4 to C2, suggesting that the crystallite thickness, L_{200}, has increased from ∼24 Å at P4 to ∼40 Å at C2 and thereafter is unchanged (C2−C10).

Scanning electron microscopy (SEM) images shown in Figure 3, of raw switchgrass stem (A and B) and hybrid poplar wood (C and D), clearly show significant differences in their cell appearances generally observed for comparison of grasses and hardwoods.[50−52] Switchgrass parenchyma cells, which comprise approximately 55% of stems, have large average cell diameters with thin cell walls typical of grasses,[50,53] while the xylem fiber cells that comprise 53−55% of the mature wood of hybrid poplar[51] exhibit smaller average cell diameters with thicker cell walls (Figure 3A and C). The texture and thickness of the cell walls observed with SEM can be used to assist in analysis of the SANS patterns. The inner surfaces of the hybrid poplar cell walls are less well-defined than the smooth inner surfaces of switchgrass cells (Figure 3B and D). Analysis of the SEM images indicates that the average diameter of switchgrass cells (∼25 μm) is about 2 to 3 times larger than hybrid poplar cells (∼10 μm), and the cell walls of hybrid poplar (∼1 μm) are at least 5 times thicker than those of switchgrass. Switchgrass cell wall thickness was estimated to be at most 0.2 μm from Figure 3B (scale bar 2.0 μm).

Chemical composition and enzymatic hydrolysis results, measured during the entire dilute acid pretreatment reaction performed for the SANS and WAXD analysis, are shown in Figures 4 and 5, respectively. Reduction in the hemicellulose or

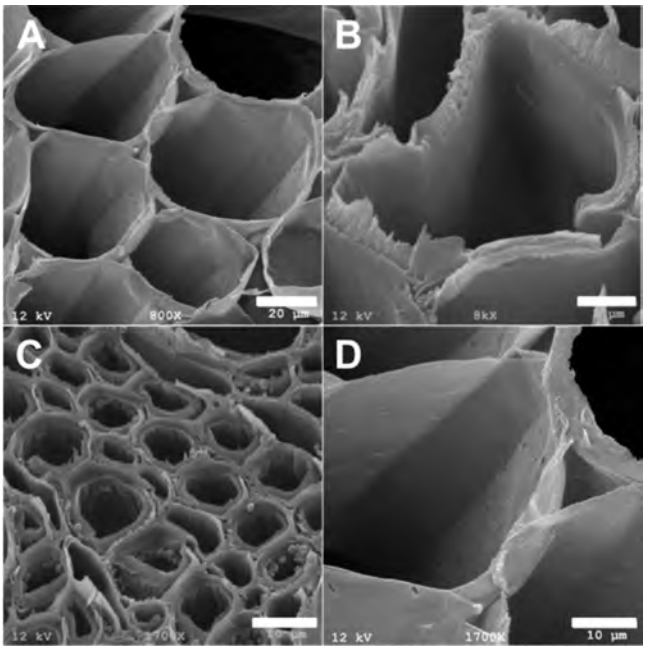

Figure 3. Scanning electron microscopy (SEM) images of parenchyma cells of raw switchgrass stem (A and B) and xylem fiber cells of hybrid poplar wood (C and D). The scale bar for panel A is 20 μm; panel B is 2 μm; and panels C and D are 10 μm.

xylan content (Figure 4B) initiates at 125 °C, but a significant decrease is only observed from 150 °C during the dilute acid pretreatment reaction. Hemicellulose dissolution and subsequent removal during rinsing occurs at a similar rate for both switchgrass and poplar prior to 2 min at 160 °C. Hemicellulose in hybrid poplar reaches undetectable quantities by 2 min at 160 °C and switchgrass hemicellulose by 20 min at 160 °C. As hemicellulose is removed, the relative concentrations of glucan and lignin (Figure 4A and C) effectively increase. Important observations in the glucan and lignin concentrations due to pretreatment include (1) similar glucan concentrations for poplar and switchgrass after pretreatment, even though initially hybrid poplar had higher glucan concentration, and (2) the relative increase in lignin concentration for hybrid poplar is more than that observed for switchgrass. Figure 5A shows enzymatic yield in glucose for switchgrass increases from 75 °C (ramp-up phase) onward, unlike hybrid poplar, where no obvious increase is visible until the constant phase (2 min at 160 °C). Furthermore, switchgrass has much higher glucose yields at ∼75 wt % as compared to ∼40 wt % for hybrid poplar. Common to both species is the saturation of enzymatic glucan yields for longer times (>10 min) at 160 °C. The most important aspect here is the lower enzymatic yield of glucose for hybrid poplar during the entire pretreatment protocol (native to 60 min at 160 °C) as compared to switchgrass, even though glucan concentration in hybrid poplar is either higher than switchgrass in the presoak phase or similar in the constant phase. Contrary to trends in the enzymatic glucose yield, enzymatic xylose yields are similar for both samples until 150 °C (ramp-up phase) at which time the xylan concentrations in the samples have already fallen dramatically low to ∼5 wt %. In the constant phase, determination of enzymatic xylose yield per xylan becomes meaningless, because xylan concentrations in the washed pretreated samples are negligible (vide infra).

DOI: 10.1021/acssuschemeng.6b01803
ACS Sustainable Chem. Eng. 2017, 5, 426−435

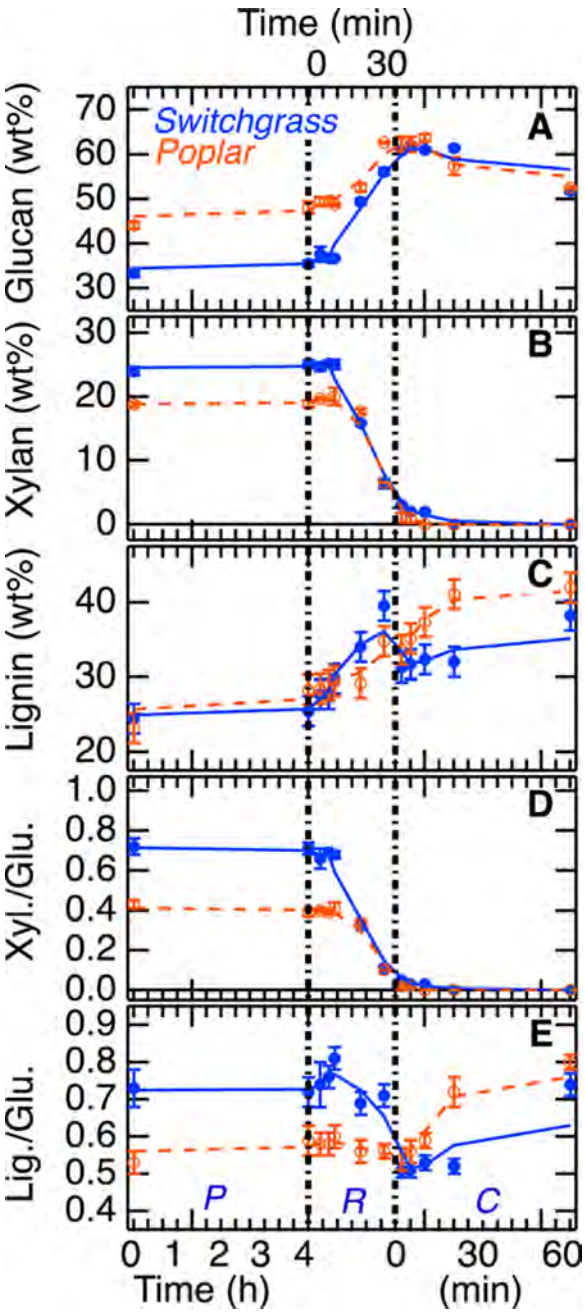

Figure 4. Chemical compositional data of switchgrass (blue dots) and hybrid poplar (red open circle) including mainly three different biomass component concentrations (wt %): glucan (A), xylan (B), and lignin (C). In addition, relative concentrations with respect to glucan concentrations are xylan/glucan (D) and lignin/glucan (E). The solid blue (switchgrass) and red dashed lines (hybrid poplar) indicate trends from the data, obtained by applying a smoothening function to the data. Refer to the Figure 2 caption for reaction time details.

DISCUSSION

Biomass structure is inherently complex with multiple components and complex spatial correlations, and such complex biological systems have been analyzed using the unified fit approach.[17,54−56] However, due to the complexity of the system, the unified fit results were not interpreted in isolation but instead as part of the body of work already performed—NMR, compositional analysis, fiber diffraction, computation, and microscopic and enzymatic digestion studies.

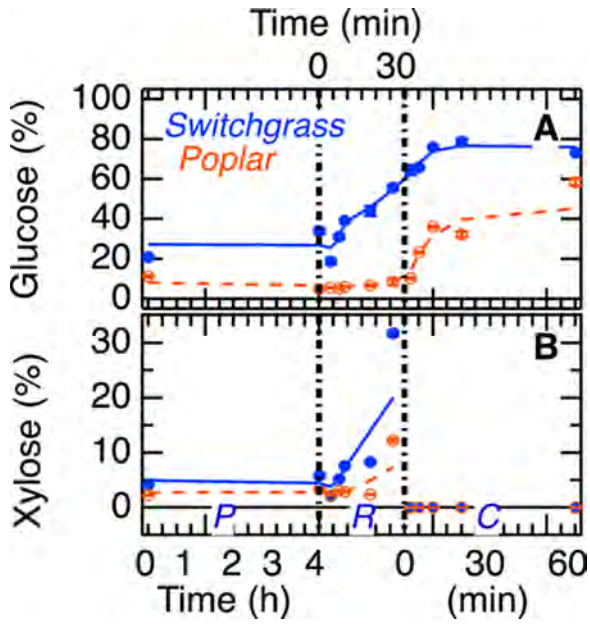

Figure 5. Enzymatic hydrolysis data of switchgrass (blue dots) and hybrid poplar (red open circles) including yields in glucose (A) and xylose (B) as a function of dilute acid pretreatment. The solid blue (switchgrass) and red dashed lines (hybrid poplar) indicate trends in the data, obtained by applying a smoothening function to the data. Switchgrass/hybrid poplar loading at 1 wt % and enzyme loading at 112.5 mg of Accellerase 1500 and 37.5 mg of Accellerase XY protein per gram of glucan and xylan (see Supporting Information for more details). Refer to the Figure 2 caption for reaction time details.

Our studies indicate that herbaceous and woody biomass samples follow a similar structural evolution during dilute acid pretreatment: (1) lignin redistribution that leads to aggregate formation, (2) enhanced crystallinity of the cellulose fibril core, and (3) significant alteration in the surface morphology or possibly porosity of the cell wall after extended duration of treatment. Structural features, such as average size of the lignin aggregates as they initially form, average size of the cellulose fibers, average size of the crystalline core of the elementary cellulose fibrils, and the cell-wall surface morphology, differ between poplar and switchgrass in their specifics. In both species, the temperature at which lignin aggregates first become visible by scattering, and the extent of growth in the average size of the lignin aggregates during the dilute acid pretreatment protocol is similar.

Cell Wall Cellulose Fibers. SEM analysis of the biomass samples shows that hybrid poplar forms thick cell walls (Figure 3B and D) compared to switchgrass. From chemical compositional results (Figure 4), initial xylan concentration in native switchgrass is ∼5 wt % higher than in hybrid poplar. But, due to xylan loss initiating earlier for switchgrass around 100 °C, the two samples have similar xylan concentrations by 125 °C. Glucan concentration for hybrid poplar is ∼10 wt % higher. The slow progression of xylan hydrolysis between 100 and 125 °C for hybrid poplar (Figure 4B) can possibly be attributed to the thick cell wall architecture because penetration of acid solution at 100 °C would be quick for a thinner cell wall like switchgrass and longer for thicker cell wall like hybrid poplar. A slight increase in temperature to 125 °C seems to be enough to overcome this difference and provide similar xylan hydrolysis rates. In the constant phase (160 °C), residual xylan concentrations remain for a longer time in switchgrass (until

DOI: 10.1021/acssuschemeng.6b01803
ACS Sustainable Chem. Eng. 2017, 5, 426−435

20 min). One plausible reason for longer time being required to dissociate xylan in switchgrass even though the cell wall is thinner can be attributed to a possible higher proportion of hemicellulose-lignin linkages.[57]

Crystalline Core of the Cellulose Fibrils. Switchgrass undergoes a 4-fold increase in the R_g associated with the crystalline core of the cellulose fibril size from 9 to 36 Å, and hybrid poplar has a slightly higher than 2-fold increase from 9 to 22 Å. This increase not only indicates that the crystalline core encompasses the entire elementary cellulose fibril[58] but also indicates coalescing of neighboring fibrils especially evident in switchgrass. The peripheral cellulose strands of the elementary cellulose fibril exhibit a lower degree of crystallinity (also referred to as para-crystalline), possibly due to the penetration of hemicellulose.[58] In this case, hemicellulose detachment from these cellulose strands and migration (or relocation) enables the growth of the crystalline form from a few central strands to outward of the elementary fibril. This can be understood as an increase of hydrogen bonding between cellulose strands, due to a lack of competition from hemicellulose for hydrogen bonds. Initially, until 10 min at 160 °C, the growth in the crystalline core of the cellulose fibrils (see Figure 2B) is similar and small. A clear difference is visible only after 10 min at 160 °C as a steep increase in the cellulose fibril size for switchgrass. Structural evolution during the initial stages is due to the disruption process of the hemicellulose-cellulose hydrogen bonding. In the ramp-up phase, increasing temperature causes a small, gradual increase in the fibril size as hemicellulose (see Figure 2B) begins to detach from the cellulose strands. We initially observe similar growth trends in the crystalline core of the elementary cellulose fibrils because hemicellulose forms hydrogen bonds to cellulose in both switchgrass and hybrid poplar. Increased temperature promotes depolymerization (acid hydrolysis) of these detached hemicelluloses into smaller oligosaccharides that now dissolve easily and therefore are lost during the rinsing process. This is consistent with a reduction in the xylan concentration in the ramp-up phase (Figure 4B). Further, crystallite thickness obtained from WAXD for a subset of the constant phase switchgrass samples (Table 1) is consistent with the crystalline fibril diameters obtained by SANS. Tables S1 and S2 list the crystalline fibril diameter (primary d) obtained by SANS and Table 1, the crystallite thickness obtained by WAXD (L_{200}). These observations are consistent with the reported 4-fold reduction of glucan chain length of poplar and switchgrass cellulose after 10 min of dilute-acid pretreatment as measured by gel permeation chromatography.[59] This reduction in chain length may facilitate recrystallization and aggregate formation, resulting in the increase of lateral fiber aggregate dimensions calculated from ^{13}C NMR by spectral fitting, which approximately doubles by 10 min residence time.

From 10 min onward to 60 min at 160 °C, the increase in the crystalline cellulose fibril diameter of switchgrass is larger than a single elementary cellulose fibril,[58] which indicates neighboring crystalline fibrils coalescing. This pronounced coalescence in switchgrass cellulose fibrils is not apparent in hybrid poplar. We believe this is due to differences in the type and proportions of cellulose crystalline forms (allomorph) found in herbaceous and woody biomass, which exhibit different propensity to crystallize and susceptibility to enzymatic hydrolysis.[60] Fiber diffraction studies are underway to address this key difference.

Initially Observed Lignin Aggregate Size. The average size of the lignin aggregates as they initially appear is 90 Å for switchgrass and 55 Å for hybrid poplar. The smaller average size observed for hybrid poplar lignin aggregates is attributed to the intrinsic structural differences between herbaceous versus woody biomass feedstock. Hemicellulose of switchgrass, a typical grass, is mainly arabinoxylan. In lignified grass cell walls, the ferulic and *p*-coumaric acids are covalently linked by ester bonds to the arabinose of the arabinoxylan. These ferulic and *p*-coumaric acids are also linked through ester bonds to proteins and lignin, generating a cross-linked network between the lignin and hemicellulose.[61,62] The reported range of lignin content of switchgrass (17−18%)[7] is lower than that reported for hybrid poplar (20−30%).[3] However, it has been established through studies with UV microspectrometry and enzymatic digestion that cells of warm-weather grasses like switchgrass, particularly those from unlignified tissues, also contain large amounts of ferulic acid and coumaric acids and their dimers esterified to arabinoxylan polysaccharides but not attached to polymeric lignin. These phenolic acid−polysaccharide complexes inhibit enzymatic degradation but can be removed by hydrolysis of the ester bonds by acid, alkali, or esterase pretreatment.[50,53] Switchgrass and hybrid poplar have different distributions of monomeric units in their lignins. In addition, differences extend beyond guaiacyl-to-syringyl ratios (G:S), such as the presence of hydroxyphenyl (H), *p*-coumaric ester, and ferulic acid ester units in switchgrass versus *p*-hydroxybenzoate unit in hybrid poplar. The untreated hybrid poplar sample has an S/G ratio of 1.2[63] typical of poplars (reported to range from 1.3−2.2[3,64]) that is higher than the S/G ratio of 0.8 for the untreated switchgrass,[62] typical of these species (ratio range of 0.4−0.7[7,65]). An S/G ratio greater than 1 implies a higher fraction of aryl ether linkages (i.e., β-*O*-4 and α-*O*-4) and an equivalently lower fraction of the more stable, condensed type of linkages (i.e., 4-O-5, 5-5, phenylcoumaran, etc.). As a result, larger sized lignin aggregates are formed in switchgrass during the temperature ramp-up of the dilute acid pretreatment.[62]

Surface Morphology Transitions of the Cell Wall. The surface morphology of the micron-sized cell walls exhibit diffuse surfaces for hybrid poplar samples until 10 min at 160 °C before a transition to a smooth surface. In contrast, for the same pretreatment protocol, switchgrass exhibits a transition in the surface morphology from smooth-to-rough after 20 min at 160 °C. Importantly, the thickness of hybrid poplar cell walls is larger than the maximum dimension observed in SANS, and it is therefore plausible that gradual variation in the composition and density (packing) from the inner to the outer cell wall surface leads to the observation of a diffuse surface in SANS. Conversely, smooth surfaces imply a sharp, well-defined boundary. Dilute acid pretreatment appears to alter poplar cell wall morphology from diffuse (such as in a thick layer with density gradient) to a sharp, well-defined, and smooth interface. The thin cell walls of switchgrass transition from a smooth surface to a rough surface, possibly with more porosity after 20 min at 160 °C.

Similar Structural Trends. First, lignin aggregates appear between 125 and 150 °C. Second, the average size of lignin aggregates doubles (90 to 200 Å for switchgrass and 55 to 130 Å for hybrid poplar) during the same temperature course of the dilute acid pretreatment protocol (Figure 1). Various explanations have been proposed to explain lignin aggregation, primarily thermal transitions, solubilization and precipitation, and/or depolymerization and repolymerization mechanisms. Despite the exact mechanisms, factors such as the spatial distribution of lignin, lignin monomer distribution, lignin

DOI: 10.1021/acssuschemeng.6b01803
ACS Sustainable Chem. Eng. 2017, 5, 426−435

monomer linkage distribution, and hemicellulose-lignin linkages can be expected to influence lignin aggregate size. Identification and quantification of the hemicellulose-lignin linkages are not yet available. In particular, our data suggest a higher S/G ratio exhibits lower activation energy for lignin aggregation.

Structural Features for Optimum Cellulose Digestion. The most interesting results from our enzymatic hydrolysis studies (see Figure 5) have been how the morphological differences observed at the molecular level correlate to the significantly higher glucose yields from switchgrass during the entire dilute acid pretreatment, which resemble those reported by earlier studies comparing these two feed stocks.[66] Enzymatic glucose yields are ∼15−20 wt % higher from switchgrass than hybrid poplar in their native state as well as for samples in the constant temperature phase of pretreatment. In the ramp-up phase, the trends differ. Enzymatic glucose yield for switchgrass increases at a constant rate from 50 °C to 10 min at 160 °C, while the yield for hybrid poplar ramps up only from 2 min at 160 °C. After an initial steep increase for hybrid poplar from 2 to 10 min at 160 °C, the increase in the enzymatic glucose yields significantly slows down. From 10 to 60 min at 160 °C, enzymatic glucose yields for hybrid poplar continue to increase, but they remain constant for switchgrass. Until 10 min at 160 °C is reached, the crystalline core diameters of the cellulose fibrils are the same between the two samples, so this does not explain why enzymatic glucose yields from hybrid poplar would be ∼15−20 wt % lower. The thick architecture of the secondary cell walls of hybrid poplar probably plays a significant role in reducing enzyme access, and therefore enzymatic glucose yields in the ramp-up phase. In addition, the smaller lignin aggregates formed in hybrid poplar could be covering a larger surface area of the cellulose fibrils and could impede the cellulase enzyme as it moves along the cellulose strands during hydrolysis resulting in lower glucose yields. Interestingly, for switchgrass, enzymatic glucose yields saturate after 10 min at 160 °C, which is when the crystalline core diameter undergoes a steep increase indicating the onset of coalescence. Conversely, the enzymatic glucose yields for hybrid poplar, which does not indicate signs of coalescence, continue to increase slowly. These trends suggest that the changes in crystalline core and lignin aggregate diameters could have a small influence on enzymatic glucose yields, they mainly suggest that cellulose fibril accessibility (i.e., surface morphology transitions) is a more likely determining factor in enzymatic glucose yields.

CONCLUSION

We have successfully used small-angle neutron scattering and wide-angle X-ray diffraction studies to probe structural and morphological changes in herbaceous and woody biomass and observed differing recalcitrance behavior to dilute acid pretreatment. The results demonstrate that dilute acid pretreatment causes (1) lignin aggregate formation and redistribution, (2) growth in the crystalline core of the cellulose fibrils, and (3) transitions in the cell wall surface morphology. Notably, following a 2-fold increase in the crystalline core of the cellulose fibrils in both types of biomass, after 10 min at 160 °C, the crystalline core increased 4-fold for switchgrass implying coalescence of neighboring crystalline cellulose fibrils. Lignin aggregate formation was first observed between 125 and 150 °C but with switchgrass forming much larger average sizes. However, the larger lignin aggregates did not correlate with enzyme inhibition as might have been expected, as glucose yields were higher for switchgrass than for hybrid poplar. Surface morphology of the micron-sized cell walls was observed to transition from smooth to rough surfaces for switchgrass as compared to diffuse to smooth surfaces for hybrid poplar, implying a greater increase in cellulosic surface area accessible to enzymes for switchgrass. Combined with the accompanying enzymatic digestion studies, these structural and morphological changes during dilute acid pretreatment suggest that cellulose accessibility is the decisive factor in increasing glucose yields, while cellulose crystallinity and lignin aggregation play lesser roles. These discoveries offer valuable insights to improving and optimizing current biomass deconstruction processes for bioethanol production by providing molecular structural information on the underlying changes to the cell wall structure that result in the subsequent increases in glucose yields targeted by empirical development of pretreatments and choice of bioenergy crops.

ASSOCIATED CONTENT

Supporting Information

The Supporting Information is available free of charge on the ACS Publications website at DOI: 10.1021/acssuschemeng.6b01803.

Descriptive details of sample preparation, small-angle neutron scattering and wide angle scattering techniques and enzymatic hydrolysis from the Methods and Materials section and two figures (SANS secondary regime plot and WAXD profiles) and two tables (Unified Fit results for switchgrass and hybrid poplar samples) from the Results section (PDF)

AUTHOR INFORMATION

Corresponding Authors

*E-mail: pingalis@ornl.gov.
*E-mail: urbanvs@ornl.gov.
*E-mail: evansb@ornl.gov.

ORCID

Sai Venkatesh Pingali: 0000-0001-7961-4176
William T. Heller: 0000-0001-6456-2975
Barbara R. Evans: 0000-0002-2574-2567

Notes

The authors declare no competing financial interest.

ACKNOWLEDGMENTS

Switchgrass and hybrid poplar samples, cell wall compositional data, and enzymatic sugar yields were obtained through a collaborative agreement with the BioEnergy Science Center (BESC) funded by DOE Office of Science, Office of Biological and Environmental Rsearch and located at the Oak Ridge National Laboratory, Oak Ridge, Tennessee. This research was funded by the DOE Office of Science, Office of Biological and Environmental Research under the Genomic Science Program (FWP ERKP752). Neutron scattering research conducted at the Bio-SANS instrument, a DOE Office of Science, Office of Biological and Environmental Research resource, used resources at the High Flux Isotope Reactor, a DOE Office of Science, Scientific User Facility operated by the Oak Ridge National Laboratory.

DOI: 10.1021/acssuschemeng.6b01803
ACS Sustainable Chem. Eng. 2017, 5, 426−435

REFERENCES

(1) Himmel, M. E.; Ding, S.-Y.; Johnson, D. K.; Adney, W. S.; Nimlos, M. R.; Brady, J. W.; Foust, T. D. Biomass Recalcitrance: Engineering Plants and Enzymes for Biofuels Production. *Science* **2007**, *315*, 804−807.

(2) Lynd, L. R.; Cushman, J. H.; Nichols, R. J.; Wyman, C. E. Fuel Ethanol from Cellulosic Biomass. *Science* **1991**, *251*, 1318−1323.

(3) Sannigrahi, P.; Ragauskas, A. J.; Tuskan, G. A. Poplar as a feedstock for biofuels: A review of compositional characteristics. *Biofuels, Bioprod. Biorefin.* **2010**, *4*, 209−226.

(4) Hegar, G. Texas State Energy Conservation Office: Forests for Fuel. http://seco.cpa.state.tx.us/energy-sources/biomass/forests.php (accessed November 21, 2016).

(5) Bouton, J. Improvement of Switchgrass as a Bioenergy Crop. In *Genetic Improvement of Bioenergy Crops*; Vermerris, W., Ed.; Springer: New York, 2008; pp 309−345.

(6) Bouton, J. H. Molecular breeding of switchgrass for use as a biofuel crop. *Curr. Opin. Genet. Dev.* **2007**, *17*, 553−558.

(7) David, K.; Ragauskas, A. J. Switchgrass as an energy crop for biofuel production: A review of its ligno-cellulosic chemical properties. *Energy Environ. Sci.* **2010**, *3*, 1182−1190.

(8) Union of Concerned Scientists: How Biopower Works. http://www.ucsusa.org/clean_energy/technology_and_impacts/energy_technologies/how-biomass-energy-works.html (accessed November 21, 2016).

(9) McMillan, J. D. Pretreatment of Lignocellulosic Biomass. In *Enzymatic Conversion of Biomass for Fuels Production*, Himmel, M. E., Baker, J. O., Overend, R. P., Eds.; ACS Symposium Series, American Chemical Society: Washington, DC, 1994; pp 292−324.

(10) Trajano, H. L.; Wyman, C. E. Fundamentals of Biomass Pretreatment at Low pH. In *Aqueous Pretreatment of Plant Biomass for Biological and Chemical Conversion to Fuels and Chemicals*, First ed.; Wyman, C. E., Ed.; John Wiley & Sons: London, 2013; pp 103−128.

(11) Wyman, C. E.; Dale, B. E.; Balan, V.; Elander, R. T.; Holzapple, M. T.; Sierra Ramirez, R.; Ladisch, M. R.; Mosier, N. D.; Lee, Y. Y.; Gupta, R.; Thomas, S. R.; Hames, B. R.; Warner, R.; Kumar, R. Comparative Performance of Leading Pretreatment Technologies for Biological Conversion of Corn Stover, Poplar Wood, and Switchgrass to Sugars. In *Aqueous Pretreatment of Plant Biomass for Biological and Chemical Conversion to Fuels and Chemicals*, First ed.; Wyman, C. E., Ed.; John Wiley & Sons: London, 2013; pp 239−259.

(12) Mosier, N.; Wyman, C.; Dale, B.; Elander, R.; Lee, Y. Y.; Holtzapple, M.; Ladisch, M. Features of promising technologies for pretreatment of lignocellulosic biomass. *Bioresour. Technol.* **2005**, *96*, 673−686.

(13) Foston, M.; Ragauskas, A. J. Biomass Characterization: Recent Progress in Understanding Biomass Recalcitrance. *Ind. Biotechnol.* **2012**, *8*, 191−208.

(14) Davison, B. H.; Parks, J.; Davis, M. F.; Donohoe, B. S. Plant Cell Walls: Basics of Structure, Chemistry, Accessibility and the influence on Conversion. In *Aqueous Pretreatment of Plant Biomass for Biological and Chemical Conversion to Fuels and Chemicals*, First ed.; Wyman, C. E., Ed.; John Wiley & Sons: London, 2013; pp 23−24.

(15) Gao, D.; Haarmeyer, C.; Balan, V.; Whitehead, T. A.; Dale, B. E.; Chundawat, S. P. Lignin triggers irreversible cellulase loss during pretreated lignocellulosic biomass saccharification. *Biotechnol. Biofuels* **2014**, *7*, 175.

(16) Li, H.; Pu, Y.; Kumar, R.; Ragauskas, A. J.; Wyman, C. E. Investigation of lignin deposition on cellulose during hydrothermal pretreatment, its effect on cellulose hydrolysis, and underlying mechanisms. *Biotechnol. Bioeng.* **2014**, *111*, 485−492.

(17) Pingali, S. V.; Urban, V. S.; Heller, W. T.; McGaughey, J.; O'Neill, H.; Foston, M.; Myles, D. A.; Ragauskas, A.; Evans, B. R. Breakdown of Cell Wall Nanostructure in Dilute Acid Pretreated Biomass. *Biomacromolecules* **2010**, *11*, 2329−2335.

(18) Martínez-Sanz, M.; Gidley, M. J.; Gilbert, E. P. Application of X-ray and neutron small angle scattering techniques to study the hierarchical structure of plant cell walls: A review. *Carbohydr. Polym.* **2015**, *125*, 120−134.

(19) Lee, I.; Evans, B. R.; Woodward, J. The mechanism of cellulase action on cotton fibers: evidence from atomic force microscopy. *Ultramicroscopy* **2000**, *82*, 213−221.

(20) Zhang, Y.-H. P.; Lynd, L. R. Toward an aggregated understanding of enzymatic hydrolysis of cellulose: Noncomplexed cellulase systems. *Biotechnol. Bioeng.* **2004**, *88*, 797−824.

(21) Norgren, M.; Edlund, H.; Wagberg, L. Aggregation of Lignin Derivatives under Alkaline Conditions. Kinetics and Aggregate Structure. *Langmuir* **2002**, *18*, 2859−2865.

(22) Vainio, U.; Maximova, N.; Hortling, B.; Laine, J.; Stenius, P.; Simola, L. K.; Gravitis, J.; Serimaa, R. Morphology of Dry Lignins and Size and Shape of Dissolved Kraft Lignin Particles by X-ray Scattering. *Langmuir* **2004**, *20*, 9736−9744.

(23) Donohoe, B. S.; Decker, S. R.; Tucker, M. P.; Himmel, M. E.; Vinzant, T. B. Visualizing lignin coalescence and migration through maize cell walls following thermochemical pretreatment. *Biotechnol. Bioeng.* **2008**, *101*, 913−925.

(24) Irvine, G. M. The significance of the glass transition of lignin in thermomechanical pulping. *Wood Sci. Technol.* **1985**, *19*, 139−149.

(25) Salmén, L. Viscoelastic properties of in-situ lignin under water-saturated conditions. *J. Mater. Sci.* **1984**, *19*, 3090−3096.

(26) Petridis, L.; Schulz, R.; Smith, J. C. Simulation Analysis of the Temperature Dependence of Lignin Structure and Dynamics. *J. Am. Chem. Soc.* **2011**, *133*, 20277−20287.

(27) Kalluri, U. C.; Yin, H.; Yang, X.; Davison, B. H. Systems and synthetic biology approaches to alter plant cell walls and reduce biomass recalcitrance. *Plant Biotechnol. J.* **2014**, *12*, 1207−1216.

(28) Poovaiah, C. R.; Nageswara-Rao, M.; Soneji, J. R.; Baxter, H. L.; Stewart, C. N. Altered lignin biosynthesis using biotechnology to improve lignocellulosic biofuel feedstocks. *Plant Biotechnol. J.* **2014**, *12*, 1163−1173.

(29) Fu, C.; Mielenz, J. R.; Xiao, X.; Ge, Y.; Hamilton, C. Y.; Rodriguez, M.; Chen, F.; Foston, M.; Ragauskas, A.; Bouton, J.; Dixon, R. A.; Wang, Z.-Y. Genetic manipulation of lignin reduces recalcitrance and improves ethanol production from switchgrass. *Proc. Natl. Acad. Sci. U. S. A.* **2011**, *108*, 3803−3808.

(30) Esteghlalian, A.; Hashimoto, A. G.; Fenske, J. J.; Penner, M. H. Modeling and optimization of the dilute-sulfuric-acid pretreatment of corn stover, poplar and switchgrass. *Bioresour. Technol.* **1997**, *59*, 129−136.

(31) Schell, D.; Farmer, J.; Newman, M.; McMillan, J. Dilute-sulfuric acid pretreatment of corn stover in pilot-scale reactor. *Appl. Biochem. Biotechnol.* **2003**, *105*, 69−85.

(32) Foston, M.; Hubbell, C.; Davis, M.; Ragauskas, A. Variations in Cellulosic Ultrastructure of Poplar. *BioEnergy Res.* **2009**, *2*, 193−197.

(33) Lynn, G. W.; Heller, W.; Urban, V.; Wignall, G. D.; Weiss, K.; Myles, D. A. A. Bio-SANS–A dedicated facility for neutron structural biology at Oak Ridge National Laboratory. *Phys. B* **2006**, *385−386*, 880−882.

(34) Ilavsky, J.; Jemian, P. R. Irena: tool suite for modeling and analysis of small-angle scattering. *J. Appl. Crystallogr.* **2009**, *42*, 347−353.

(35) Belina, G.; Urban, V.; Straube, E.; Pyckhout-Hintzen, W.; Kluppel, M.; Heinrich, G. Microscopic deformation of filler particles in rubber under uniaxial deformation. *Macromol. Symp.* **2003**, *200*, 121−128.

(36) Cullity, B. D.; Stock, S. R. *Elements of X-Ray Diffraction*, 3rd ed.; Prentice-Hall Inc.: Upper Saddle River, NJ, 2001.

(37) Klug, H. P.; Alexander, L. E. *X-ray Diffraction Procedures for Polycrystalline and Amorphous Materials*, 2nd ed.; John Wiley & Sons: New York, 1974.

(38) DeMartini, J. D.; Studer, M. H.; Wyman, C. E. Small-scale and automatable high-throughput compositional analysis of biomass. *Biotechnol. Bioeng.* **2011**, *108*, 306−312.

(39) Sluiter, A.; Hames, B.; Ruiz, R.; Scarlata, C.; Sluiter, J.; Templeton, D.; Crocker, D. Determination of Structural Carbohydrates and Lignin in Biomass. In *Laboratory Analytical Procedure (LAP)*, Revised 2012; NREL/TP-510-42618, National Renewable Energy Laboratory: Golden, CO, 2008.

DOI: 10.1021/acssuschemeng.6b01803
ACS Sustainable Chem. Eng. 2017, 5, 426−435

(40) DeMartini, J. D.; Wyman, C. E. Changes in composition and sugar release across the annual rings of Populus wood and implications on recalcitrance. *Bioresour. Technol.* **2011**, *102*, 1352−1358.
(41) Studer, M. H.; DeMartini, J. D.; Brethauer, S.; McKenzie, H. L.; Wyman, C. E. Engineering of a high-throughput screening system to identify cellulosic biomass, pretreatments, and enzyme formulations that enhance sugar release. *Biotechnol. Bioeng.* **2010**, *105*, 231−238.
(42) Beaucage, G. Approximations Leading to a Unified Exponential Power-Law Approach to Small-Angle Scattering. *J. Appl. Crystallogr.* **1995**, *28*, 717−728.
(43) Beaucage, G. Small-Angle Scattering from Polymeric Mass Fractals of Arbitrary Mass-Fractal Dimension. *J. Appl. Crystallogr.* **1996**, *29*, 134−146.
(44) Pingali, S. V.; Urban, V. S.; Heller, W. T.; McGaughey, J.; O'Neill, H. M.; Foston, M.; Myles, D. A.; Ragauskas, A. J.; Evans, B. R. SANS study of cellulose extracted from switchgrass. *Acta Crystallogr., Sect. D: Biol. Crystallogr.* **2010**, *66*, 1189−1193.
(45) Schmidt, P. W.; Avnir, D.; Levy, D.; Hohr, A.; Steiner, M.; Roll, A. Small-angle x-ray scattering from the surfaces of reversed-phase silicas: Power-law scattering exponents of magnitudes greater than four. *J. Chem. Phys.* **1991**, *94*, 1474−1479.
(46) Hubbell, C. A.; Ragauskas, A. J. Effect of acid-chlorite delignification on cellulose degree of polymerization. *Bioresour. Technol.* **2010**, *101*, 7410−7415.
(47) Kawakatsu, T.; Tanaka, H.; Koizumi, S.; Hashimoto, T. Computer simulation of reaction-induced self-assembly of cellulose via enzymatic polymerization. *J. Phys.: Condens. Matter* **2006**, *18*, S2499−S2512.
(48) Tanaka, H.; Koizumi, S.; Hashimoto, T.; Kurosaki, K.; Kobayashi, S. Self-Assembly of Synthetic Cellulose during in-Vitro Enzymatic Polymerization Process As Studied by a Combined Small-Angle Scattering Method. *Macromolecules* **2007**, *40*, 6304.
(49) Wada, M.; Kwon, G. J.; Nishiyama, Y. Structure and Thermal Behavior of a Cellulose I-Ethylenediamine Complex. *Biomacromolecules* **2008**, *9*, 2898.
(50) Akin, D. E. Grass lignocellulose: strategies to overcome recalcitrance. *Appl. Biochem. Biotechnol.* **2007**, *137−140*, 3−15.
(51) Mellerowicz, E. J.; Baucher, M.; Sundberg, B.; Boerjan, W. Unravelling cell wall formation in the woody dicot stem. *Plant Mol. Biol.* **2001**, *47*, 239−274.
(52) Ong, R. G.; Chundawat, S. P. S.; Hodge, D. B.; Keskar, S.; Dale, B. E. Linking Plant Biology and Pretreatment: Understanding the Structure and Organization of the Plant Cell Wall and Interactions with Cellulosic Biofuel Production. In *Plants and BioEnergy*, McCann, M. C., Buckeridge, M. S., Carpita, N. C., Eds.; Advances in Plant Biology, Springer: New York, 2014; pp 231−253.
(53) Anderson, W. F.; Akin, D. E. Structural and chemical properties of grass lignocelluloses related to conversion for biofuels. *J. Ind. Microbiol. Biotechnol.* **2008**, *35*, 355−366.
(54) Imel, A. E.; Naskar, A. K.; Dadmun, M. D. Understanding the Impact of Poly(ethylene oxide) on the Assembly of Lignin in Solution toward Improved Carbon Fiber Production. *ACS Appl. Mater. Interfaces* **2016**, *8*, 3200−3207.
(55) Hu, N.; Borkar, N.; Kohls, D.; Schaefer, D. W. Characterization of porous materials using combined small-angle X-ray and neutron scattering techniques. *J. Membr. Sci.* **2011**, *379*, 138−145.
(56) Beaucage, G. Toward Resolution of Ambiguity for the Unfolded State. *Biophys. J.* **2008**, *95*, 503−509.
(57) Hatakeyama, H.; Hatakeyama, T. Thermal Properties of Isolated and in-situ Lignin. In *Lignin and Lignans*, Heitner, C., Dimmel, D. R., Schmidt, J. A., Eds.; Advances in Chemistry, CRC Press: Boca Raton, FL, 2010; pp 301−319.
(58) Ding, S.-Y.; Himmel, M. E. The Maize Primary Cell Wall Microfibril: A New Model Derived from Direct Visualization. *J. Agric. Food Chem.* **2006**, *54*, 597−606.
(59) Foston, M.; Ragauskas, A. J. Changes in lignocellulosic supramolecular and ultrastructure during dilute acid pretreatment of Populus and switchgrass. *Biomass Bioenergy* **2010**, *34*, 1885−1895.
(60) Chundawat, S. P. S.; Bellesia, G.; Uppugundla, N.; da Costa Sousa, L.; Gao, D.; Cheh, A. M.; Agarwal, U. P.; Bianchetti, C. M.; Phillips, G. N.; Langan, P.; Balan, V.; Gnanakaran, S.; Dale, B. E. Restructuring the Crystalline Cellulose Hydrogen Bond Network Enhances Its Depolymerization Rate. *J. Am. Chem. Soc.* **2011**, *133*, 11163−11174.
(61) de Oliveira, D. M.; Finger-Teixeira, A.; Rodrigues Mota, T.; Salvador, V. H.; Moreira-Vilar, F. C.; Correa Molinari, H. B.; Craig Mitchell, R. A.; Marchiosi, R.; Ferrarese-Filho, O.; Dantas dos Santos, W. Ferulic acid: a key component in grass lignocellulose recalcitrance to hydrolysis. *Plant Biotechnol. J.* **2015**, *13*, 1224−1232.
(62) Samuel, R.; Pu, Y.; Raman, B.; Ragauskas, A. Structural Characterization and Comparison of Switchgrass Ball-milled Lignin Before and After Dilute Acid Pretreatment. *Appl. Biochem. Biotechnol.* **2010**, *162*, 62−74.
(63) Pu, Y.; Cao, S.; Studer, M.; Wyman, C.; Ragauskas, A. J. *Abstracts of Papers*, 239th National Meeting of the American Chemical Society, San Francisco, CA, March 21−25, 2010; American Chemical Society: Washington, DC, 2010; AGFD 18.
(64) Jung, S.; Foston, M.; Sullards, M. C.; Ragauskas, A. J. Surface Characterization of Dilute Acid Pretreated Populus deltoides by ToF-SIMS. *Energy Fuels* **2010**, *24*, 1347−1357.
(65) Hu, Z.; Sykes, R.; Davis, M. F.; Charles Brummer, E.; Ragauskas, A. J. Chemical profiles of switchgrass. *Bioresour. Technol.* **2010**, *101*, 3253−3257.
(66) Chung, Y.-C.; Bakalinsky, A.; Penner, M. Enzymatic saccharification and fermentation of xylose-optimized dilute acid-treated lignocellulosics. *Appl. Biochem. Biotechnol.* **2005**, *124*, 947−961.
(67) Langan, P.; Petridis, M.; O'Neill, H. M.; Pingali, S. V.; Foston, M.; Nishiyama, T.; Schulz, R.; Lindner, B.; Hanson, B. L.; Harton, S.; Heller, W. T.; Urban, V.; Evans, B. R.; Gnanakaran, S.; Ragauskas, A. J.; Smith, J.; Davison, B. H. Common processes drive the thermochemical pretreatment of lignocellulosic biomass. *Green Chem.* **2014**, *16*, 63−68.

DOI: 10.1021/acssuschemeng.6b01803
ACS Sustainable Chem. Eng. 2017, 5, 426−435